Experimental investigation of non-Newtonian droplet splitting mechanism in a cross-flow type microfluidic device

DHRUVKUMAR H WANKAWALA and PRANAB K MONDAL*

Microfluidics and Microscale Transport Processes Laboratory, Department of Mechanical Engineering, Indian Institute of Technology Guwahati, Guwahati 781039, India
e-mail: dhruvkumar@iitg.ac.in; pranabm@iitg.ac.in

Abstract. The dynamics of non-Newtonian shear-thinning (carboxymethyl cellulose-CMC solution) droplet splitting with permanent and partial obstructions are experimentally investigated using a high-speed experimental framework in a microfluidic T-junction divergence. Four sequential stages of shear-thinning droplet splitting are found: squeezing, transition, pinch-off, and rupture. The role of various flow and fluid parameters (CMC concentrations, flow ratio, and droplet size) on the splitting dynamics is investigated with the help of flow regime maps. The dynamics of droplet neck thinning and the intriguing phenomenon of satellite droplet formation are further investigated at distinct CMC concentrations. The present study aims to enhance comprehension of the phenomenon of rapid droplet splitting, which has greater outreach in biofluids-based applications.

Keywords. Microfluidics; multiphase flow; splitting; non-Newtonian fluid.

1. Introduction

In recent times, droplet-based microfluidics has emerged as a well-established technique for various fields and applications, including chemical analysis, droplet emulsification, food processing, drug delivery, mixing, and point-of-care diagnostics, to name a few [1]. Comparatively, droplet microfluidics possess advantages such as high controllability, responsiveness, and precise sample volume handling over conventional droplet manipulation tools. Currently, microfluidics is the demanding ground for several droplet-based operations for instant generation, splitting, merging, transportation, mixing, separation, etc. Among these, droplet splitting refers to the process of dividing a mother droplet into two sister droplets, either symmetrical or asymmetrical, within a microfluidic device [2].

In general, active and passive methods are used to achieve droplet manipulation. In active methods, external energy in terms of a magnetic field, acoustic, electrical, optical, and mechanical is involved for controlled and precise droplet manipulation [3]. On the other hand, the passive method employs droplet manipulation by modulating the geometry of the microfluidic device, interfacial tension, flow rate, and viscosity of the liquid-liquid phase [4]. Passive droplet modulation can be obtained by number of microfluidic systems, such as cross-flow, co-flow, and flow-focusing geometries [5]. We employed the most common T-junction (cross-flow microfluidic structure) to investigate the droplet splitting phenomenon in the present work.

Several studies have been devoted to the droplet splitting process at a T-junction through analytical analysis, experimental investigations, and numerical simulations. Albeit, most of the studies have explored splitting dynamics for Newtonian fluids ensuing three typical types: no-splitting, permanent splitting, and partial splitting [6]. However, studies explaining the droplet splitting dynamics for non-Newtonian fluids remain to be explored [7]. It is essential to mention that non-Newtonian fluids such as blood, grease, salivary fluids, and paint are of prime importance in multiple scientific disciplines, such as chemistry, medicine, and biology. Therefore, in the present study, we unreel the splitting dynamics of shear-thinning carboxymethyl cellulose (CMC) fluid in a microfluidic T-junction. We experimentally investigate the droplet splitting event for permanent and partial obstructions by employing different CMC concentrations, two-phase fluid flow ratio, and the size of the mother droplet. Subsequently, we explain the flow pattern map of droplet splitting types under distinct two-phase fluid flow rates and CMC concentrations. In the end, we show the evolution of droplet neck thinning and the emergence of satellite droplets attributed to the shear-thinning rheology.

---

*For correspondence

2. Materials and methods

Figure 1 depicts the experimental configuration used in the present study for conducting droplet splitting operations. It consists of two syringe pumps, a microfluidic device, an inverted microscope (Make: Leica), and a high-speed camera (Make: Phantom). We positioned a microfluidic device under an inverted microscope connected to a high-speed camera with a high-resolution window of 1920×1080 pixels^2. Videos are captured at 1000 frames per second. The schematic of a microfluidic device is shown in the zoomed-in view of figure 1. We fabricated a microfluidic device using the soft lithography method. The master is prepared in negative photoresist SU-8 on a silicone substrate employing UV light through photo mask with proposed T-junction geometry. The PDMS (Polydimethylsiloxane, Sylgard 184) is poured onto master to gain negative replica of microfluidic geometry, and finally, the PDMS replica is plasma bonded with glass. The microfluidic device has a cross-section of $100\,\mu$m (width) $\times$ $100\,\mu$m (height).

It is evident from figure 1 that the microfluidic device includes three major sections: a first T-junction (T_1) for mother droplet formation, a straight passageway, and a second T-junction (T_2) for droplet splitting. Two immiscible fluids, i.e., continuous and dispersed phases, are injected into the microfluidic device via syringe pumps from inlets A and B, respectively. Both the immiscible liquids meet at the first T-junction (see figure 1) to form a train of droplets. Then, the droplet train travels through a microfluidic passage and reaches second T-junction (see figure 1), where the mother droplet splits into two symmetric sister droplets.

In the present study, we used mustard oil as a continuous phase fluid with density and viscosity of $902\,\text{kg/m}^3$ and

0.06 Pa.s, respectively. At the same time, the different CMC concentrations ($c = 0.2\%$–0.6%) are used as a dispersed phase fluid whose rheological properties are mentioned in table 1. Note that we employ flow ratio $Q(Q_d/Q_c)$ in between 0.1 and 1.5. Here, Q_c and Q_d referred to continuous and dispersed phase flow rates, respectively. In addition, we employed capillary number Ca $\left(Ca = \frac{\mu_c(Q_c + Q_d)}{w_c^2 \sigma}\right)$ in the range of 0.05 to 0.22. Here, μ_c, w_c, and σ represent the viscosity of continuous phase fluid, the width of the channel, and the interfacial tension, respectively. Further, we normalize splitting time with capillary time $T_c = (\rho_c w_c^3/\sigma)^{0.5}$ to speak for droplet neck thinning variation.

3. Results and discussion

3.1 *The process of shear-thinning droplet splitting in permanent and partial type*

It may be mentioned here that, based on the capillary number (Ca), flow ratio (Q), and dimensionless mother droplet length (L_o/w_c), the event of droplet splitting can be classified into three types: (a) no-splitting, (b) permanent splitting, and (c) partial splitting. Here, the no-splitting case refers to a scenario in which a droplet upon reaching the point of divergence (at the T-junction), does not experience any mode of splitting. While the distinction between permanent and partial splitting is based on whether there is a visible tunnel or gap between the droplet interface and the microchannel wall. In the following discussion, we provide a comprehensive analysis of the splitting dynamics associated with shear-thinning rheology, considering permanent and partial scenarios.
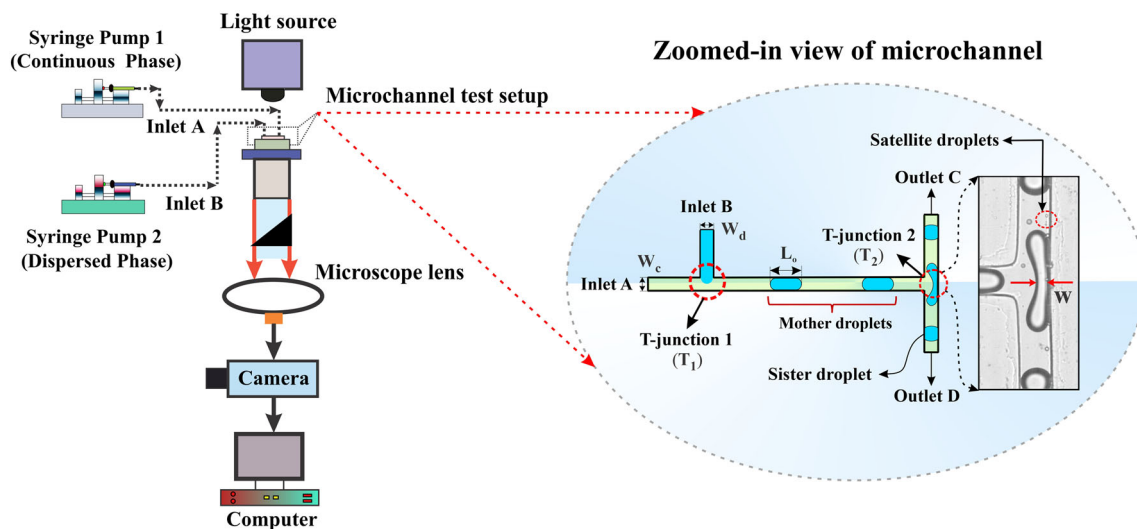

Figure 1. Schematic of the experimental setup used to perform the droplet splitting operation. Zoomed-in view provides a detailed depiction of the microfluidic device and the physical parameters involved in the current investigation.

Table 1. Rheological properties of shear-thinning fluid (CMC solution) used in the present study.

CMC concentration	Flow consistency index $m(\text{Pa.s}^n)$	Flow behaviour index (n)	Interfacial tension $\sigma(\text{mN.m}^{-1})$
0.2%	0.065	0.90	5
0.4%	0.130	0.82	4.82
0.6%	0.202	0.75	4.78

In figure 2, we show the permanent splitting case following four stages of droplet neck evolution: squeezing, transition, pinch-off, and rupture, respectively. From figure 2(a), it is evident that the droplet upon arriving at the T-junction divergence, hinders the motion of a continuous-phase fluid. In addition, as seen in figure 2, there is no observable tunnel between the droplet tip and the channel wall. Consequently, during the squeezing stage, the upstream continuous fluid exerts enormous pressure on the droplet rear (see figure 2a). In the transition stage, the above-stated squeezing pressure is balanced by the interfacial force. However, the non-existence of a tunnel enables squeezing pressure to mostly dominate in the transition stage, too (see figure 2b). Subsequently, the ongoing process of elongation rapidly diminishes the droplet neck in the pinch-off stage (see figure 2c) and, in the end, detaches in the rupture stage (see figure 2d), by breaking the mother droplet into two sister droplets.

Analogous to permanent splitting, partial splitting occurs in four stages of droplet neck evolution: squeezing, transition, pinch-off, and rupture, respectively. Figure 3 clearly demonstrates the development of a tunnel between the droplet tip and sidewalls in the event of partial splitting. Initially, the droplets undergo a squeezing stage during which the primary cause of neck thinning is the sustained application of squeezing pressure (refer to figure 3a). Afterward, the process of neck thinning progresses into a transitional stage (refer to figure 3b), wherein the squeezing pressure is counteracted by the viscous shear of the continuous fluid (due to the opening of tunnel). This interaction results in a little deceleration in the rate of droplet neck thinning (w/w_c). Upon closer examination of figure 3, it is visible that the tunnel widen more in the transition stage compared to the squeezing stage, followed by a gradual reduction in width during the pinch-off stage. Besides, the neck thinning rate increases in the pinch-off stage compared to the previous two stages i.e., squeezing and transition, owning to the effect of continuous phase flow rate, tunnel contraction, and the arrival of an upcoming droplet (refer to figure 3c). In the rupture stage, a cylindrical droplet neck formed as a consequence of ongoing stretching in the direction perpendicular to the main channel gets fully
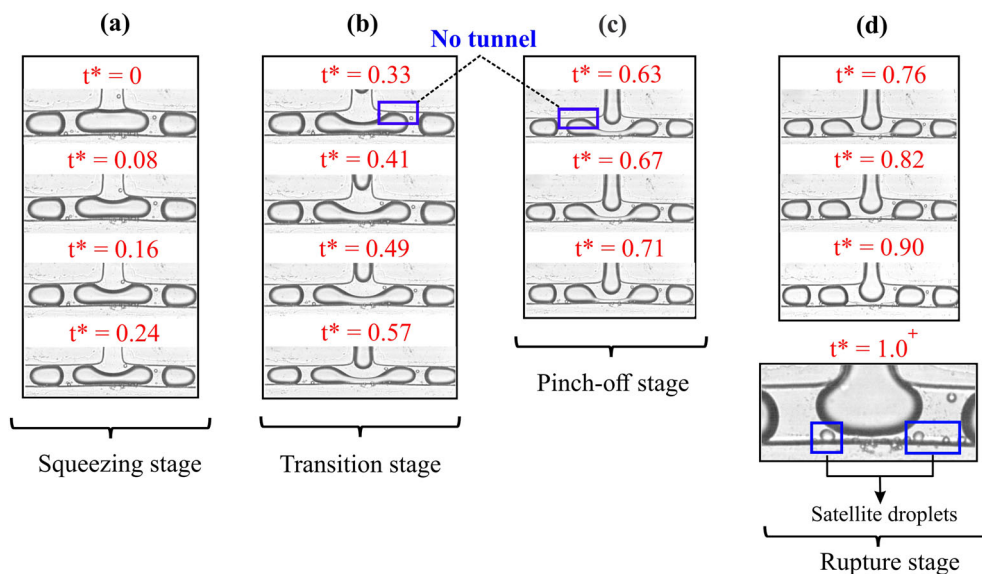

(a) $t^* = 0$, $t^* = 0.08$, $t^* = 0.16$, $t^* = 0.24$ — Squeezing stage

(b) No tunnel, $t^* = 0.33$, $t^* = 0.41$, $t^* = 0.49$, $t^* = 0.57$ — Transition stage

(c) $t^* = 0.63$, $t^* = 0.67$, $t^* = 0.71$ — Pinch-off stage

(d) $t^* = 0.76$, $t^* = 0.82$, $t^* = 0.90$, $t^* = 1.0^+$ — Satellite droplets — Rupture stage

Figure 2. Temporal evolution of permanent type droplet splitting phenomenon in a microfluidic device. $c = 0.2\%, n = 0.9,$ $Ca = 0.2, Q_d = 0.22\,\text{ml/hr}, Q_c = 0.17\,\text{ml/hr}, L_o/w_c = 4$. (a)–(d) showcase four stages observed during droplet splitting termed as squeezing, transition, pinch-off and rupture. $t^* = t/T$ represent the dimensionless time of droplet splitting phenomena. Here, t represent the instantaneous time, while T signifies the total time required for droplet detachment.

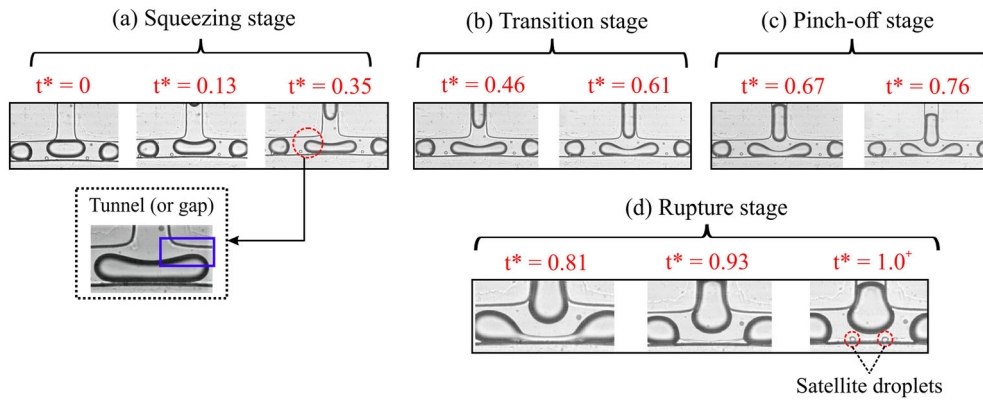**Figure 3.** Temporal evolution of partial type droplet splitting phenomenon in a microfluidic device. $c = 0.2\%, n = 0.9$, $Ca = 0.126, Q_d = 0.16 \, \text{ml/hr}, Q_c = 0.17 \, \text{ml/hr}, L_o/w_c = 2.8$. (a)–(d) showcase four stages observed during droplet splitting: squeezing, transition, pinch-off, and rupture.

detached (refer to figure 3d). At the instant of a complete droplet splitting, the emergence of satellite droplets can be noticed due to capillary instability, which will be further examined in section 3.4.

3.2 *Splitting pattern of shear-thinning droplets*

In figures 4(a, b), we show the flow pattern map illustrating the shear-thinning droplet splitting types i.e., no splitting, permanent and partial splitting, under distinct combinations of continuous (Q_c) and dispersed phase (Q_d) flow rates for two different CMC concentrations, 0.2% and 0.6%. It can be seen from figures 4(a, b) that the no-splitting type is noticed when the dispersed phase flow rate remains low and constant while keeping a sufficiently high continuous phase flow rate. However, gradual increment in Q_d compared to Q_c configures partial splitting type at T-junction divergence. While further increase in Q_d subsequently evolves partial splitting into permanent splitting type.

Interestingly, we discover that, at lower CMC concentration *i.e.*, $c = 0.2\%$, partial splitting is more evident than permanent splitting (see figure 4a). With the increase in CMC concentration *i.e.*, $c = 0.6\%$, a regime with partial splitting decreases, although it remains greater as compared with permanent splitting (see figure 4b). From the viewpoint of mother droplet length (L_o/w_c), we noticed that when $L_o/w_c < 2$, the droplet does not split but instead passes through the left or right sister branch owing to the random disturbance. An increase of Q_d achieves a partial obstruction case when $2 < L_o/w_c \leq 3$, while permanent case for $L_o/w_c > 3$.

3.3 *Neck thinning dynamics of shear-thinning droplets*

Figure 5(a, b) demonstrate the neck thinning evolution in shear-thinning droplets at various lengths of mother droplet (L_o/w_c), for CMC concentrations of 0.2% and 0.6%. It is
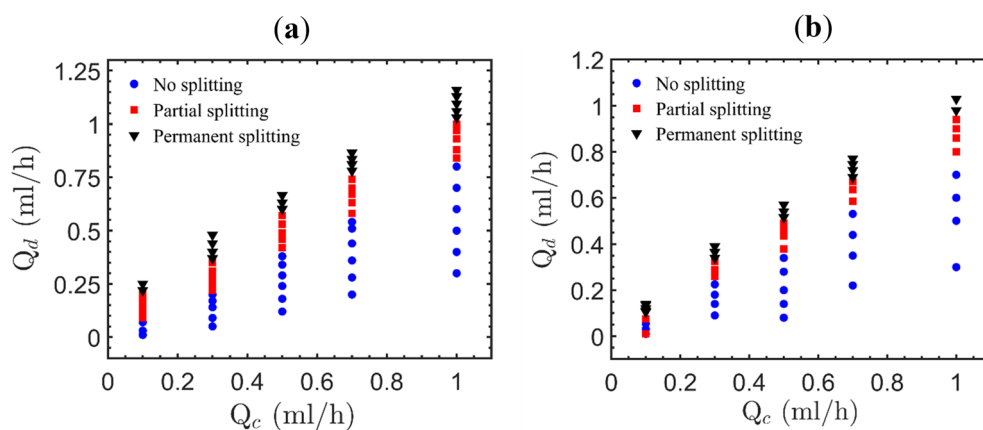

Figure 4. Flow pattern map of droplet splitting types (no-splitting, permanent, and partial) in a microfluidic T-junction; (a) $c = 0.2\%$, and (b) $c = 0.6\%$.
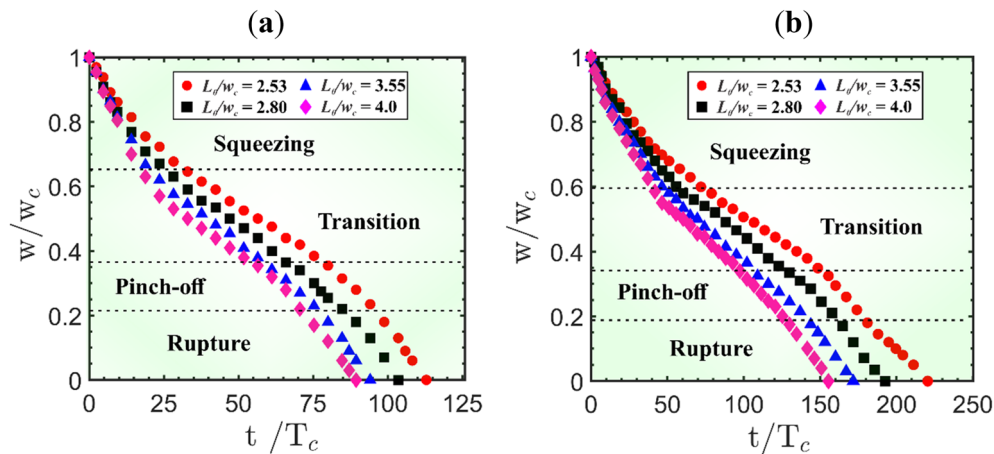
Figure 5. Evolution of non-dimensional droplet neck width for different mother droplet lengths in case of, (a) $c = 0.2\%$, (b) $c = 0.6\%$.

apparent from figure 5(a, b) that the dimensionless neck width (w/w_c) continuously decreases until splitting occurs for all droplet lengths under consideration. Besides, it is observed that the droplet of larger size or length (permanent case, $L_o/w_c = 3.55, 4.0$) exhibit a shorter splitting time in comparison to relatively smaller size droplet (partial case, $L_o/w_c = 2.53, 2.80$). One significant factor contributing to this behaviour is the direct correlation between the widening of the tunnel and the size of the mother droplet. The experimental results indicate that there is a decrease in the tunnel width as the length of the droplet increases. This implies that the extent of leakage of the surrounding continuous-phase fluid through a tunnel is greater for smaller droplet lengths compared to bigger ones. Undoubtedly, the presence of tunnel has a significant impact on the accumulation of squeezing pressure. It is worth noting that the tunneling effect becomes less pronounced when the droplet size falls within the range of $3 < L_o/w_c < 4$ (i.e., longer length droplets, permanent case). Consequently, neck thinning process is accelerated, leading to a reduction in the total splitting time required for longer length droplets, as depicted in figures 5(a, b).

Alternatively, the spacing between successive droplets plays a vital role in the process of neck thinning and the overall duration of droplet splitting. For example, the inter-droplet spacing (between two subsequent droplets) is greater for smaller droplets compared to larger droplets. The end result is the acceleration of neck thinning process for longer droplets. Another important aspect for consideration is the effect of CMC concentration on the droplet necking. With increased CMC concentration, the enhanced shear-thinning properties enable higher droplet elongation in the transverse direction to the main channel. This sort of response is more significant in transition and thereafter stages as the interfacial tension and droplet viscous stress, play an essential role on the account of shear-thinning rheology. This is also the reason why total splitting time

achieved is greater for the 0.6% CMC concentration scenario in comparison to the 0.2% instance, given the identical droplet size (refer to figures 5a, b).

3.4 *Dynamics of satellite droplet formation*

It should be noted that satellite droplets are formed at the end of the rupture stage in both permanent and partial splitting. At this juncture, we would like to comment on several observations regarding satellite droplet formation. It is well known that satellite droplets form because of capillary instabilities. Pertaining to capillary instabilities, Driessen *et al* [8] reported that the instability in a longer viscous thread could be understood from the convective instability, conversely, a short viscous thread can be explained by absolute instability. Additionally, the dynamics behind thread rupture can be analogized with the liquid jet formed in flow focusing systems. Concerning this, Eggers and Villermaux [9] revealed that depending upon the fluid viscosity, size, and shape of thread, it may break into either a single droplet (stable) or multiple droplets (unstable).

In this work, we examined the dynamics of satellite droplet formation pertaining to the phenomenon of partial splitting. It is evident from figure 6 that, in the context of partial splitting, the satellite droplets exhibit discernible differences in their breakdown characteristics at lower and higher CMC concentrations. At lower CMC concentration (0.2%), thread elongation of a droplet in a transverse direction to the main channel is shorter; accordingly, it produces only two satellite droplets (see figure 6). Nevertheless, at high CMC concentration (0.6%), thread elongation is higher, and therefore, we observed multiple satellite droplet formation (see figure 6). In figure 7(a), we show the variation of thread elongation length (L/w_c) for different CMC concentrations during partial splitting. It is clearly seen from figure 7(a) that thread length is much
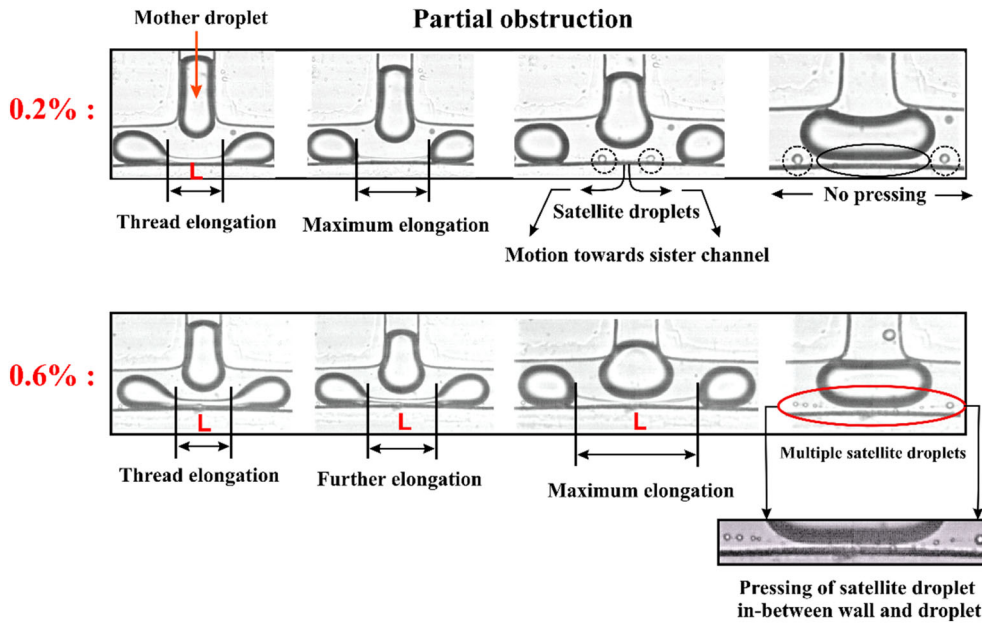
Figure 6. Development of droplet thread elongation in rupture stage with the generation of satellite droplets for partial obstruction case; $c = 0.2\%$ and 0.6%.

smaller for 0.2% concentration than for 0.6% CMC concentration. We further show in figure 7(b) the variation of thread elongation length (L/w_c) for permanent splitting. As for the permanent splitting case, we observed multiple satellite droplets at both lower and higher CMC concentrations.

Now, we comment on the trajectory of satellite droplets subsequent to the splitting process. For the partial case, we observed that a shorter thread (at 0.2% CMC concentration) allows satellite droplets to move towards the sister channels before the arrival of the next droplet. Instead, satellite droplets break very close to the next droplet in case of a longer thread (at 0.6% CMC concentration) and thus make themselves incapable of moving away from the wall towards sister channels. Hence, these satellite droplets are likely pressed between the next droplet and the microfluidic channel wall. Moreover, these satellite droplets do not coalesce with either of the other near satellite droplet or the next mother droplet but may imbalance the uniformity of the subsequent droplet breakup. It is critical to note that the variation in thread elongation is purely due to the shear-thinning property of the dispersed phase and the interfacial tension with mustard oil. Thus, the rupture behaviour (or satellite droplet formation) may change owing to a change in the physical properties of both the continuous and dispersed phase fluids.
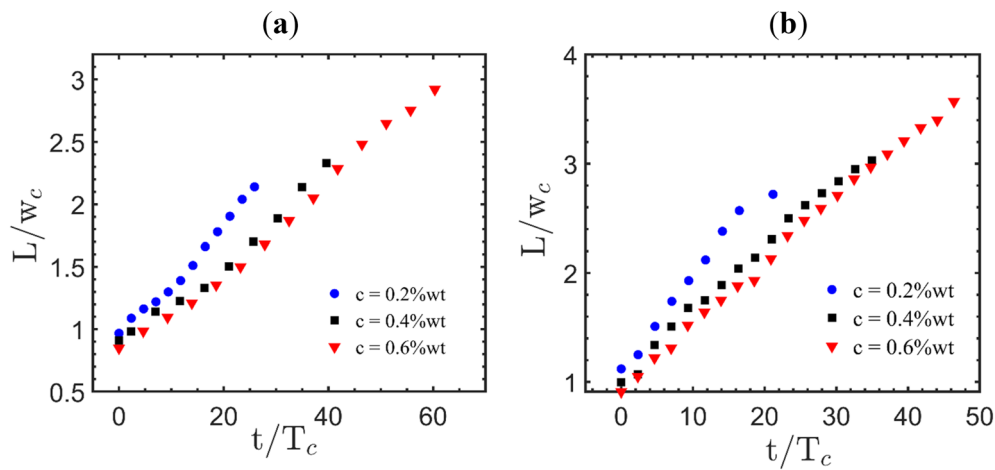

Figure 7. Effect of CMC concentration on the development of thread elongation length with dimensionless time for, (a) partial splitting; $Q = 0.8, L_o/w_c = 2.5$, (b) permanent splitting; $Q = 1.2, L_o/w_c = 4.0$.

4. Conclusions

In this study, we explored the dynamics of non-Newtonian shear-thinning droplet splitting in a T-junction of a microfluidic device. Firstly, we investigated the dynamics of permanent and partial splitting ensuing four stages: squeezing, transition, pinch-off, and rupture. Further, we demonstrated the flow regime maps for different CMC concentrations and the continuous and dispersed flow rates. We found that the partial splitting regime is the largest regime observed for CMC concentrations under consideration. Besides, we observed that the shear-thinning droplet does not split when dimensionless droplet length (L_o/w_c) is less than 2. At the same time, the partial and permanent splitting occurs with the dimensionless droplet length ranging in-between 2 to 3 and 3 to 4. On the other hand, we revealed the neck thinning dynamics of permanent and partial splitting with different dimensionless droplet lengths for 0.2% and 0.6% CMC concentrations. At last, we explained the satellite droplet formation and the evolution of thread elongation length for partial splitting. It is found that, for the partial splitting, a higher concentration of CMC (0.6%) exhibit more thread elongation in a transverse direction because of the shear-thinning property and thereby produces multiple satellite droplets in contrast to a two satellite droplet formed at a lower CMC concentration (0.2%). We believe that the present experimental study can provide fundamental understanding associated with non-Newtonian rheology and can be useful for further experimental and numerical investigation incorporating complex microfluidic geometries and fluid rheology.

Abbreviation

CMC   Carboxymethyl cellulose

List of symbols

T_1	T-junction for droplet formation process
T_2	T-junction for droplet splitting process
c	CMC concentration
Q	Flow ratio
Q_d	Dispersed phase flow rate
Q_c	Continuous phase flow rate
Ca	Capillary number
μ_c	Viscosity of continuous fluid
w_c	Width of continuous phase channel
σ	Interfacial tension
T_c	Capillary time
ρ_c	Density of continuous fluid
w_d	Width of dispersed phase channel
L_o	Length of mother droplet
L_o/w_c	Dimensionless mother droplet length
m	Flow consistency index
n	Flow behaviour index
w	Droplet neck width
w/w_c	Dimensionless droplet neck width
t^*	Dimensionless droplet splitting time
t	Instantaneous splitting time
T	Total splitting time
L	Thread elongation length
L/w_c	Dimensionless thread elongation length

References

[1] Teh S Y, Lin R, Hung L H and Lee A P 2008 Droplet microfluidics. *Lab Chip.* 8(2): 198–220

[2] Link D R, Anna S L, Weitz D A and Stone H A 2004 Geometrically mediated breakup of drops in microfluidic devices. *Phys. Rev. Lett.* 92(5): 054503

[3] Shyam S, Mondal P K and Mehta B 2021 Magnetofluidic mixing of a ferrofluid droplet under the influence of a time-dependent external field. *J. Fluid Mech.* 917: 1–29

[4] Zhu P and Wang L 2017 Passive and active droplet generation with microfluidics: a review. *Lab Chip.* 17(1): 34–75

[5] Baroud C N, Gallaire F and Dangla R 2010 Dynamics of microfluidic droplets. *Lab Chip.* 10(16): 2032–2045

[6] Jullien M C, Tsang M C, Cohen M J, Menetrier C and Tabeling P 2009 Droplet breakup in microfluidic T-junctions at small capillary numbers. *Phys. Fluids* 21(7): 1–7

[7] Ma Y, Zhu C, Fu T, Ma Y and Li H Z 2021 Dynamics of non-Newtonian droplet breakup with partial obstruction in microfluidic Y-junction. *Chem. Eng. Sci.* 240: 116696

[8] Driessen T, Jeurissen R, Wijshoff H, Toschi F and Lohse D 2013 Stability of viscous long liquid filaments. *Phys. Fluids.* 25(6): 062109

[9] Eggers J and Villermaux E 2008 Physics of liquid jets. *Rep. Prog. Phys.* 71(3): 036601